Emission Control Science and Technology (2018) 4:90–102
https://doi.org/10.1007/s40825-018-0083-9

Efficient Solution of Washcoat Diffusion-Reaction Problem for Real-Time Simulations

Santhosh R. Gundlapally[1] · Ryan Dudgeon[1] · Syed Wahiduzzaman[1]

Received: 30 October 2017 / Revised: 21 December 2017 / Accepted: 15 January 2018 / Published online: 17 February 2018

Abstract

As countries around the globe adapt more stringent emissions standards set by Real Driving Emissions (RDE) legislation, mathematical models are becoming ever more widely used as plant models for devising vehicle control strategies. It is important for the model to run on Hardware-in-Loop (HIL) and engine control unit (ECU) systems which have significantly less computational power and memory than modern personal computers. Washcoat diffusion limitations play a very important role in the efficient design of a catalytic converter. Numerical solution of aftertreatment models that include diffusion-reaction equations in the washcoat are computationally demanding. There are several simplified approaches proposed in the literature for the solution of diffusion-reaction equations in the washcoat to avoid the computational demand of the full numerical solution. In this paper, we use the recently proposed asymptotic solution and compare the results with that of the full numerical solution for the following aftertreatment reactor models with both single- and dual-layer washcoat configurations for the practical range of operating conditions; three-way catalyst (TWC), diesel oxidation catalyst (DOC), Selective Catalytic Reduction (SCR), and ammonia slip catalyst (ASC). These reactor models are constructed using published kinetic mechanisms and represent the global kinetics mechanisms (including non-linear reaction orders and inhibition functions) commonly used in the aftertreatment modeling community. We also discuss the importance of adaptive mesh, quasi-steady state assumption, and occurrence of concentration jumps in the simulation of aftertreatment reactors.

Keywords Washcoat · Diffusion · Asymptotic · Dual-layer · Real time

Abbreviations

$a_n^{(l)}$	active site density of reaction n in layer l (mol − site/m^3)
$A_k^{(l)}$	active site density for coverage k in layer l (mol − site/m^3)
C_{pg}	heat capacity of bulk gas (J/(Kg K))
C_p^l	heat capacity of washcoat layer l (J/(Kg K))
$C_{p,sb}$	heat capacity of substrate (J/(Kg K))
D_h	hydraulic diameter of channel (m)
$D_{i,m}$	diffusivity of species i in the mixture (m^2/s)
$D_{i,eff}^{(l)}$	effective diffusivity of species i in washcoat layer l (m^2/s)
$D_{i,kn}^{(l)}$	Knudsen diffusivity of species i in washcoat layer l (m^2/s)
$\boldsymbol{D}_{\mathbf{inv}}^{(l)}$	diagonal matrix of dimensionless effective diffusion resistances in washcoat layer l.
$d_p^{(l)}$	pore diameter of washcoat layer l (m)
$f^{(l)}$	volume fraction of layer l
f_{sb}	volume fraction of substrate
f_{vd}	void fraction of reactor
h	heat transfer coefficient (J/(m^2 s K))
h_x	external heat transfer coefficient (J/(m^2 s K))
k_i	mass transfer coefficient of species i (m/s)
$\boldsymbol{K}$	diagonal matrix of dimensionless mass transfer coefficients
L	length of reactor (m)
MW_i	molecular weight of species i (kg/mol)
n_{rxns}	total number of reactions
n_{sp}	total number of species
R_g	gas constant (J/(mol K))
$r_n^{(l)}$	nth reaction rate in layer l (mol/(mol − site s))
R_i^l	ith species rate in layer l (kg/(m^3 s))
$\boldsymbol{R}^{(l)}$	vector of species rates in layer l
$s_{i,n}$	stoichiometric coefficient of species i in reaction n

✉ Santhosh R. Gundlapally
s.gundlapally@gtisoft.com

[1] Gamma Technologies, 601 Oakmont Lane, Westmont, IL 60559, USA

S	specific area per reactor volume (m^{-1})
S_x	external surface area per reactor volume (m^{-1})
t	time (s)
T_g	gas temperature (K)
T_s	solid temperature (K)
T_x	external temperature (K)
u	average gas velocity (m/s)
x	position through the washcoat thickness (m)
z	axial position (m)
δ^l	effective thickness of washcoat layer l (m)
$\varepsilon^{(l)}$	porosity of layer l
$\Delta H_n^{(l)}$	heat of n^{th} reaction in layer l (J/mol)
$\theta_k^{(l)}$	surface coverages of species k in layer l
$\lambda^{(l)}$	thermal conductivity of layer l (J/(m s K))
λ_{sb}	thermal conductivity of substrate (J/(m s K))
Λ_s	effective thermal conductivity of reactor (J/(m s K))
ρ_g	density of bulk gas (kg/m^3)
ρ_s	density of gas within washcoat (kg/m^3)
$\rho^{(l)}$	density of washcoat layer l (kg/m^3)
ρ_{sb}	density of substrate (kg/m^3)
$\sigma_{k,n}$	stoichiometric coefficient for coverage k in reaction n
ψ_s	effective heat capacity of reactor ($J/(m^3\ K)$)
$\omega_{g,i}$	mass fraction of species i in the bulk gas
$\boldsymbol{\omega_g}$	vector of species mass fractions in the bulk gas
ω_i	mass fraction of species i in the washcoat
$\boldsymbol{\omega}$	vector of species fractions in the washcoat
$\omega_{s,i}$	mass fraction of species i at the washcoat/channel surface
$\boldsymbol{\omega_s}$	vector of species fractions at the washcoat/channel surface

1 Introduction

Monolithic catalytic converters are widely used in the exhaust aftertreatment applications for their several advantages over the packed bed reactors [1]. Figure 1 shows the overview of various physical and chemical processes occurring inside a catalytic monolithic reactor channel; reactants diffuse from the bulk gas phase to the washcoat surface (external mass transfer), reactants diffuse through the washcoat pores (pore diffusion), surface reactions occur at the active sites (adsorption/reaction/desorption), and finally, products diffuse back through the washcoat into the bulk gas phase. Depending on the geometric, kinetic, and operating conditions, one or a combination of these steps may control the conversion rate of reactant pollutants. For example, as the inlet gas temperature increases, the controlling step may change from a kinetics-controlled regime at low temperature (before light-off) to an external mass transfer-controlled regime at high temperatures. In between these two extreme regimes, a transition regime may exist where combination of external mass transfer and pore diffusion steps control the conversion rate of pollutants

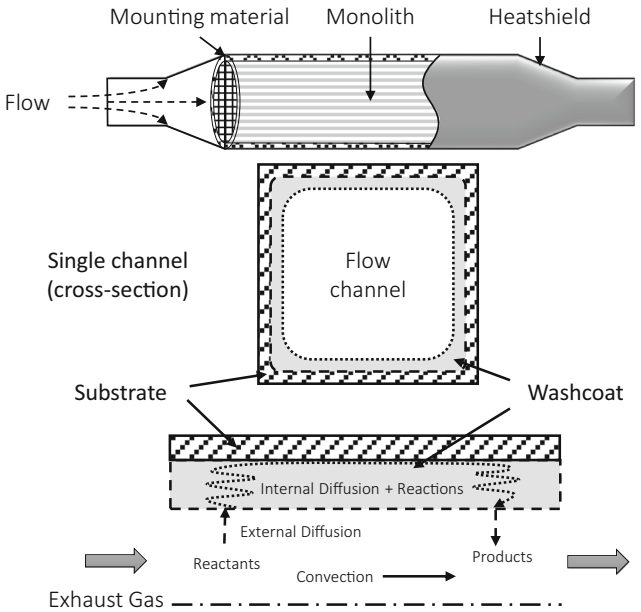

Fig. 1 Overview of important physical and chemical processes occurring in a washcoated monolith channel

[2]. Thus, pore diffusion may play an important role in the conversion rate of pollutants for some operating conditions. In addition, pore diffusion plays an important role in the design of dual layer catalysts which are designed to take advantage of pore diffusion limitations [3, 4]. The full numerical solution of the model consisting of convection-diffusion-reaction equations is computationally demanding and is suitable for offline system analysis and design, but not real-time control applications. It is possible to simulate the detailed model in real time using modern computers but not on the Hardware-in-Loop (HIL) and engine control unit (ECU) systems due to their limited computational capability. As countries around the globe are adapting more stringent emissions standards set by Real Driving Emissions (RDE) legislation, mathematical models are increasingly used as plant models for devising vehicle control strategies. For this reason, it is important to develop physics-based models that can run on HIL and ECU machines in real time. While it is possible to develop simplified models that are compatible with HIL and ECU systems for a specific kinetics mechanism [5], there is a strong need for computationally efficient models that can be used with any kinetics mechanism. Several simplified modeling approaches have been proposed to account for pore diffusion without significant computational cost of the full numerical solution. The proposed simplified approaches mainly fall into three categories: effectiveness factor [6], internal mass transfer coefficient [2, 7], and the asymptotic solution [8]. We refer the interested readers to reference [8, 9] for the detailed discussion about these three approaches. There are several papers published in the literature on the effectiveness factor and internal mass transfer

coefficient approaches [2, 7, 10, 11] but the accuracy of the asymptotic solution has not yet been demonstrated for wide range of conditions. It is argued in [8] that the asymptotic solution is easier to implement than the other solutions without ad hoc approximations and is best suited for the aftertreatment reactors where the effective diffusivity in the washcoat is on the order of 10^{-6} m^2/s. As pointed out in the original paper [8], the asymptotic solution is expected to give good results but its accuracy cannot be predicted a priori.

The main objective of this study is to assess the accuracy of asymptotic solution for a wide variety of kinetic mechanisms and practical range of operating conditions commonly encountered in the aftertreatment reactors. The paper is organized as follows: first, we present the mathematical model that is applicable to both single- and dual-layer washcoat configurations. Next, we present the equations used in the asymptotic solution. We then discuss the quasi-steady state approximation, concentration jumps, and application of adaptive mesh. Finally, we compare the asymptotic solution results with the 1 + 1D solution for different aftertreatment reactor models.

2 Mathematical Model

Detailed mathematical models of monolith reactors consist of a system of partial differential equations with highly non-linear reaction source terms. Although the numerical solution of the detailed mathematical models is possible with modern personal computers, it is not practical when the objective is to explore the parameter space, conduct optimization studies, and devise control strategies. The most widely used models of catalytic monoliths are the 1 + 1D (with one spatial dimension in the flow direction and the second spatial dimension through the washcoat thickness) and 1D (with one spatial direction in the flow direction) two-phase models. It is shown that these two-phase models capture all the qualitative features of the monolith reactor, and the quantitative predictions are also accurate for all practical purposes [12]. In the 1 + 1D model, a separate differential equation (Eq. 8) is used to resolve concentration gradients within the washcoat (i.e., captures the pore diffusion resistance) whereas in the 1D model pore diffusion resistance is either set to zero or addressed by using a simplified approach. Based on the intended application, these two-phase models can be further simplified for different limiting cases, such as infinite/zero solid phase conductivity and negligible gradients between fluid and solid phases [13].

The 1 + 1D two-phase model used in this work is described by the following conservation equations and boundary conditions:

Gas phase species:

$$f_{\mathrm{vd}} * \rho_{\mathrm{g}} * \frac{\partial \omega_{\mathrm{g,i}}}{\partial \mathrm{t}} = -f_{\mathrm{vd}} * \rho_{g} * u * \frac{\partial \omega_{\mathrm{g,i}}}{\partial \mathrm{z}} - \rho_{\mathrm{g}} * k_{\mathrm{i}} * S * \left(\omega_{\mathrm{g,i}} - \omega_{\mathrm{s,i}}\right) \quad (1)$$

Gas phase energy:

$$f_{\mathrm{vd}} * \rho_{\mathrm{g}} * C_{\mathrm{pg}} * \frac{\partial T_{\mathrm{g}}}{\partial \mathrm{t}} = -f_{\mathrm{vd}} * \rho_{\mathrm{g}} * C_{\mathrm{pg}} * u * \frac{\partial T_{\mathrm{g}}}{\partial \mathrm{z}} + h * S * \left(T_{\mathrm{s}} - T_{\mathrm{g}}\right) \quad (2)$$

Solid phase energy:

$$\psi_{\mathrm{s}} * \frac{\partial T_{\mathrm{s}}}{\partial \mathrm{t}} = \frac{\partial}{\partial \mathrm{z}}\left(\Lambda_{\mathrm{s}} * \frac{\partial T_{\mathrm{s}}}{\partial \mathrm{z}}\right) - h * S * \left(T_{\mathrm{s}} - T_{\mathrm{g}}\right) - h_{\mathrm{x}} * S_{\mathrm{x}} * \left(T_{\mathrm{s}} - T_{\mathrm{x}}\right) + \sum_{l=1}^{2} \sum_{n=1}^{n_{rxns}} \Delta H_{n}^{(\mathrm{l})} * a_{n}^{(l)} * \bar{r}_{n}^{(l)} \quad (3)$$

Where Λ_{s} and ψ_{s} are, respectively, effective thermal conductivity and effective heat capacity of solid phase, and are given by the following equations

$$\Lambda_{\mathrm{s}} = f_{\mathrm{sb}} * \lambda_{\mathrm{sb}} + \sum_{\mathrm{l}=1}^{2} f^{(l)} * \lambda^{(l)} \quad (4)$$

$$\psi_{\mathrm{s}} = f_{\mathrm{sb}} * \rho_{\mathrm{sb}} * C_{\mathrm{p,sb}} + \sum_{l=1}^{2} f^{(l)} * \rho^{(l)} * C_{\mathrm{p}}^{(l)} \quad (5)$$

$\bar{r}_{n}^{(l)}$ is the average reaction rate across the effective washcoat thickness

$$\bar{r}_{n}^{(l)} = \frac{1}{\delta^{(l)}} \int_{0}^{\delta^{(\mathrm{l})}} r_{n}^{(l)}\, \mathrm{dx} \qquad l = 1, 2 \quad (6)$$

Where the effective washcoat thickness is defined as

$$\delta^{(l)} = \frac{f^{(l)}}{S}, \qquad l = 1, 2 \quad (7)$$

The effective washcoat thickness defined as above accounts for the small additional washcoat volume in the corners of a channel and will be slightly larger than the measured value.

Initial and boundary conditions for the above differential equations are trivial and are not given here. The following equations present the species balances and boundary conditions in the washcoat layers.

Washcoat species:

$$f^{(l)} * \varepsilon^{(l)} * \rho_{\mathrm{s}} * \frac{\partial \omega_{\mathrm{i}}}{\partial \mathrm{t}} = f^{(l)} * \rho_{\mathrm{s}} * \mathrm{D}_{\mathrm{i,eff}}^{(l)} * \frac{\partial^2 \omega_{\mathrm{i}}}{\partial x^2} + R_{\mathrm{i}}^{(l)}, \qquad l = 1, 2 \quad (8)$$

$R_i^{(l)}$ is the i^{th} species rate in layer l

$$R_i^{(l)} = \mathrm{MW_i} \sum_{n=1}^{n_{rxns}} s_{i,n} * a_n^{(l)} * r_n^{(l)} \tag{9}$$

Boundary condition at the surface:

$$k_{m,i} * \rho_g * \left(\omega_{g,i} - \omega_{s,i}\right) = -\rho_s * D_{i,eff}^{(l)} * \left.\frac{\partial \omega_i}{\partial x}\right|_{x=0} \tag{10}$$

Flux continuity at the layer interface:

$$\rho_s * D_{i,eff}^{(1)} * \left.\frac{\partial \omega_i}{\partial x}\right|_{x=\delta^{(1)}-} = \rho_s * D_{i,eff}^{(2)} * \left.\frac{\partial \omega_i}{\partial x}\right|_{x=\delta^{(1)}+} \tag{11}$$

Boundary condition at the bottom of the washcoat:

$$\left.\frac{\partial \omega_i}{\partial x}\right|_{x=\delta^{(1)}+\delta^{(2)}} = 0 \tag{12}$$

Site balance:

$$A_k^{(l)} * \frac{\partial \theta_k^{(l)}}{\partial t} = \sum_{n=1}^{n_{rxns}} \sigma_{k,n} * a_n^{(l)} * r_n^{(l)} \quad l = 1, 2 \tag{13}$$

The variables used in the above equations are defined in the abbreviations section. We note that the reaction rates in the above equations are based on turnover number defined as moles reacted/(moles of active sites $\cdot s$). Volume rates are obtained by multiplying turnover rates with active site density. It is recommended to use turnover rates as they do not depend on catalyst loading and hence are easily portable to different reactors with same catalyst formulation but different catalyst loading. Turnover rates are also useful when modeling aging and poisoning of catalysts which are generally accounted for by reducing the active site density.

We note that various correlations are available in the literature to account for the entrance length effects on heat and mass transfer coefficients. It is shown in [14] that when the transverse Peclet number ($P = \frac{u * D_h^2}{16 * L * D_{i,m}}$) is less than 0.25, flow conditions in the entry region of a monolith channel have negligible effect on the exit conversion. Normally, the transverse Peclet number is less than 0.1 for the monoliths used in the automotive exhaust aftertreatment applications, and hence, we use the heat and mass transfer coefficients calculated from constant Sherwood number corresponding to a square channel shape (i.e., 2.98). Binary diffusion coefficients are calculated using the Fuller correlation based on special atomic diffusion volumes [15]

$$D_{i,j} = \frac{10^{-7} * T^{1.75} * \sqrt{\frac{1}{\mathrm{MW_i}} + \frac{1}{\mathrm{MW_j}}}}{P * \left(\left(\sum_i v_k\right)^{\frac{1}{3}} + \left(\sum_j v_k\right)^{\frac{1}{3}}\right)^2} \tag{14}$$

where $D_{i,j}$ is binary diffusion coefficient of species i in species j $\left(\mathrm{m^2}/\mathrm{s}\right)$, T is temperature (K), P is pressure (atm), MW is molecular weight $\left(\mathrm{g}/\mathrm{mol}\right)$, and v_k is atomic diffusion volumes ($\mathrm{cm^3}$) summed over all the atoms contained in diffusing species. Mixture-averaged diffusion coefficient $D_{i,m}$ is calculated from the above binary diffusion coefficients $D_{i,j}$ [16]

$$D_{i,m} = \frac{1 - \omega_i}{\sum_{\substack{j=1 \\ j \neq i}}^{nsp} \frac{X_j}{D_{i,j}}} \tag{15}$$

Effective diffusion coefficients are calculated from the above mixture-averaged diffusion coefficient, Knudsen diffusion coefficient $D_{i,kn}$, and washcoat properties

$$D_{i,eff}^{(l)} = \frac{\tau^{(l)}}{\varepsilon^{(l)}} * \left(\frac{1}{D_{i,m}} + \frac{1}{D_{i,kn}^{(l)}}\right) \tag{16}$$

$$D_{i,kn}^{(l)} = \frac{d_p^{(l)}}{3} * \sqrt{\frac{8 * R_g * T}{\pi * \mathrm{MW_i}}} \tag{17}$$

Where $\tau^{(l)}, \varepsilon^{(l)}, and\ d_p^{(l)}$ are tortuosity, porosity, and pore diameter of washcoat layer l, respectively. Molecular weight of species, $\mathrm{MW_i}$, is in kg/mol in the above equation.

3 Asymptotic Solution

Numerically coupling the washcoat diffusion-reaction equation (Eq. 8) with 1D equations at each axial location is computationally expensive. The simplest approach for avoiding computation cost of full numerical solution is to neglect the pore diffusion resistance. In the absence of pore diffusion resistance, species concentration profiles in the washcoat are constant, and integrating diffusion-reaction equation (Eq. 8) and using boundary conditions (Eqs. 10 and 12) result in the following equation for the concentration in a single layer washcoat

$$f^{(1)} * \varepsilon^{(1)} * \rho_s * \frac{d\omega_{s,i}}{dt} = S * k_i * \rho_g * \left(\omega_{g,i} - \omega_{s,i}\right) + R_i^{(1)}(\boldsymbol{\omega_s}) \tag{18}$$

where $\omega_{s,\,i}$ is the surface concentration of species i. Even though this is a reasonable approximation for the aftertreatment applications as the washcoat layers are

generally thin and highly porous, the interest in understanding the effect of pore diffusion remains strong, especially for dual-layer catalysts where pore diffusion resistance is intentionally exploited for better conversion efficiency [3, 4, 17, 18]. In this section, we present the important equations used in the asymptotic solution approach. The equations presented below are in dimensionless form as the asymptotic solution was derived based on the assumption of small dimensionless diffusion resistance. Washcoat layers are non-dimensionalized such that layer 1 occupies interval [0,1] and layer 2 occupies interval [1, 2]

$$\hat{x} = \begin{cases} \dfrac{x}{\delta^{(1)}}, & 0 \le x \le \delta^{(1)} \\ 1 + \dfrac{x-\delta^{(1)}}{\delta^{(2)}}, & \delta^{(1)} < x \le \delta^{(1)} + \delta^{(2)} \end{cases} \tag{19}$$

The following equations were derived by integrating Eq. 8 over the washcoat thickness and applying the boundary and flux conditions to determine the constants of integration. We refer the interested readers to reference [8, 9] for the detailed derivation of these equations.

3.1 Single-Layer Washcoat

The species mass fraction profile in the washcoat is given by

$$\omega = \overline{\omega} + \boldsymbol{D}_{\mathrm{inv}} * \boldsymbol{R}\left(\overline{\omega}\right) * \left[\frac{1}{6} - \frac{1}{2}(1-\hat{x})^2\right] \tag{20}$$

The species mass fraction at the surface, ω_s is determined from above equation by substituting $\hat{x} = 0$

$$\omega_s = \overline{\omega} - \frac{\boldsymbol{D}_{\mathrm{inv}} * \boldsymbol{R}\left(\overline{\omega}\right)}{3} \tag{21}$$

Then the following differential equation is solved for $\overline{\omega}$

$$\frac{\mathrm{d}\overline{\omega}}{\mathrm{dt}} = \boldsymbol{K} * \left(\omega_g - \omega_s\right) + \boldsymbol{R}\left(\overline{\omega}\right) \tag{22}$$

It can be seen from the above equations that asymptotic solution can be implemented similarly to the limiting case of zero pore diffusion resistance. With asymptotic solution $\overline{\omega}$ is solved for instead of ω_s which is a known function through Eq. 21 whereas $\overline{\omega}=\omega_s$ for the zero pore diffusion resistance. Thus, there is very little overhead associated with the asymptotic solution.

3.2 Dual-Layer Washcoat

The species mass fraction profile in the layer exposed to the channel gas (layer one) is given by

$$\omega = \overline{\omega}^{(1)} + \boldsymbol{D}_{\mathrm{inv}}^{(1)} * \boldsymbol{R}^{(1)}\left(\overline{\omega}^{(1)}\right) * \left[\frac{1}{6} - \frac{1}{2}(1-\hat{x})^2\right] + \boldsymbol{D}_{\mathrm{inv}}^{(1)} * \boldsymbol{R}^{(2)}\left(\overline{\omega}^{(2)}\right) * \left(\hat{x} - \frac{1}{2}\right) \tag{23}$$

And in layer two by

$$\omega = \overline{\omega}^{(2)} + \boldsymbol{D}_{\mathrm{inv}}^{(2)} * \boldsymbol{R}^{(2)}\left(\overline{\omega}^{(2)}\right) * \left[\frac{1}{6} - \frac{1}{2}(2-\hat{x})^2\right] \tag{24}$$

The species mass fraction ω_s at the surface is determined from Eq. 23 by substituting $\hat{x} = 0$

$$\omega_s = \overline{\omega}^{(1)} - \frac{\boldsymbol{D}_{\mathrm{inv}}^{(1)} * \boldsymbol{R}^{(1)}\left(\overline{\omega}^{(1)}\right)}{3} - \frac{\boldsymbol{D}_{\mathrm{inv}}^{(1)} * \boldsymbol{R}^{(2)}\left(\overline{\omega}^{(2)}\right)}{2} \tag{25}$$

Then the following equations are solved for $\overline{\omega}^{(1)}$ and $\overline{\omega}^{(2)}$

$$\frac{\mathrm{d}\overline{\omega}^{(1)}}{\mathrm{dt}} = \boldsymbol{K} * \left(\omega_g - \omega_s\right) + \boldsymbol{R}^{(1)}\left(\overline{\omega}^{(1)}\right) + \boldsymbol{R}^{(2)}\left(\overline{\omega}^{(2)}\right) \tag{26}$$

$$\frac{\mathrm{d}\overline{\omega}^{(2)}}{\mathrm{dt}} = \overline{\omega}^{(1)} - \overline{\omega}^{(2)} + \frac{\boldsymbol{D}_{\mathrm{inv}}^{(1)}}{6} * \boldsymbol{R}^{(1)}\left(\overline{\omega}^{(1)}\right) + \left(\frac{\boldsymbol{D}_{\mathrm{inv}}^{(1)}}{2} + \frac{\boldsymbol{D}_{\mathrm{inv}}^{(2)}}{3}\right) * \boldsymbol{R}^{(2)}\left(\overline{\omega}^{(2)}\right) \tag{27}$$

4 Numerical Solution

Method of lines (MOL) approach is widely used in the literature to discretize the partial differential equations (PDEs) presented in the Section 2. After discretizing the spatial dimension, the PDEs become ordinary differential equations (ODEs) which can be solved using any of the ODE solver packages available in the open literature. The most popular ODE solver packages like LSODI, VODE, and DASPK are based on implicit backward difference formulas (BDF) which are best suited for the stiff problems encountered in aftertreatment reactors. In this work, we used LOSDI solver package with variable order BDF method option. Note that we also need to discretize the diffusion-reaction equation (Eq. 8) along the washcoat thickness for the full numerical solution of 1 + 1D model. Numerical solution of the diffusion-reaction equation within the washcoat increases the computational cost tremendously as additional variables (for species concentrations) at transverse mesh points within the washcoat need to be solved at each axial mesh point.

4.1 Quasi-Steady State Approximation

The quasi-steady state (QSS) approximation is widely used by the reactor modeling community because it

reduces the computational time by eliminating shorter time scales associated with the small accumulation terms (time derivatives) in the gas phase species and energy and washcoat species balance equations. The system of PDEs discussed above become a system of differential algebraic equations (DAEs) after invoking the QSS approximation. It is important to note that the QSS approximation introduces additional mathematical complications when the surface concentration changes discontinuously along the reactor length. We will briefly explain here why the so-called concentration jumps cause the DAE solver failures and refer the interested user to [13] for more details on bifurcation analysis of catalytic reactors. To simplify the discussion, we assume no pore diffusion resistance in the washcoat. For this limiting case, Eq. 18 becomes the following algebraic equation after applying the QSS assumption

$$S * k_{\mathrm{i}} * \rho_{\mathrm{g}} * \left(\omega_{\mathrm{g,i}} - \omega_{\mathrm{s,i}}\right) + R_{\mathrm{i}}(\boldsymbol{\omega_{\mathrm{s}}}) = 0 \tag{28}$$

Discontinuities in surface concentrations, $\boldsymbol{\omega_{\mathrm{s}}}$, occur when the solution to the above algebraic equation reaches a limit point where the Jacobian matrix becomes singular. At the limit point, the surface concentration undergoes abrupt changes. This is illustrated in Fig. 2 which shows the bulk and surface CO concentration profiles obtained from a simulation involving the oxidation of CO in excess O_2, as would occur in diesel oxidation catalyst. The reaction rate used is

$$r = 1.183 * 10^{12} * e^{-9782/T_{\mathrm{s}}} * \frac{[\mathrm{CO}] \times [\mathrm{O_2}]}{\left(1 + 248 * e^{-615/T_{\mathrm{s}}} * [\mathrm{CO}]\right)^2}, \left(\frac{\mathrm{mol}}{\mathrm{m^3 s}}\right) \tag{29}$$

It can be seen from Fig. 2 that the discontinuity in CO surface concentration occurs at the dimensionless channel location of 0.5 where surface concentration jumps from 0.25 to 0.04%. DAE solvers struggle as the solution approaches the discontinuity and often fail as the error test forces very small time step sizes. Thus, special considerations have to be taken during the simulation to avoid integration failures due to discontinuous concentration jumps. At the minimum one needs to monitor the Jacobian matrix and use special logic to help the DAE solvers to find the solution at the limit point. The rest of the variables ($\boldsymbol{\omega_{\mathrm{g}}}$, T_{g}) do not change discontinuously because the axial derivative terms that appear in the governing equations guarantee smoothness.

4.2 Adaptive Mesh

Sharp reaction fronts where most of the reactant conversion takes place are routinely present inside the channels of monolith reactors. These reaction fronts dynamically move within the channel in response to the operating conditions and accurately resolving species concentration profiles inside a

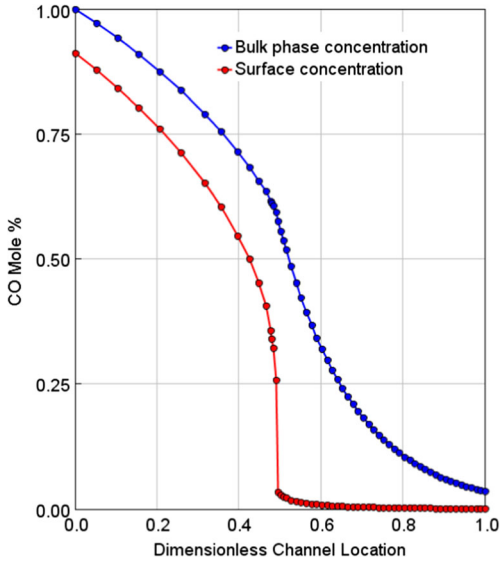

Fig. 2 Bulk and surface concentration profiles. Surface concentration profile shows an abrupt change in CO concentration at the dimensionless channel location of 0.5

reaction front is computationally challenging. An adaptive meshing method that dynamically follows the reaction fronts was proposed in [19] but this method has not seen wide spread use in the simulation of aftertreatment reactors. We believe that the aftertreatment modeling community can benefit from the discussion of this adaptive meshing technique which can offer significant benefits over the uniform fixed mesh solvers. An adaptive mesh with little computational overhead can be implemented since the solid temperature and surface coverages vary slowly with time due to their large accumulation or capacity terms whereas species concentrations and gas temperature exhibit fast dynamics due to their small accumulation terms. After applying the QSS assumption, solid temperature and coverage equations are the only equations that have explicit time derivatives. Species and gas temperature equations have only axial derivatives. Thus, it is possible to construct the problem as outer and inner integration problems. In the outer problem, time integration of solid temperature and coverages is carried out on a fixed uniform MOL mesh whereas in the inner problem integration of DAE system consisting of species and gas temperature equations is carried out on adaptive mesh. In this dual mesh strategy, LSODI solver automatically creates a spatially non-uniform mesh, just like the time integration, in accordance with the specified error tolerances. This method also works when there are multiple reaction fronts at the same time since the LSODI solver controls the axial integration error for each of the species solved and hence increases the mesh resolution wherever needed to meet the specified error tolerance. We note that this approach does not decouple or lag the variables in any way but simply takes advantage of the structure of our particular DAE system [19].

The first significant and obvious advantage of the above adaptive mesh technique over the fixed uniform mesh is that the adaptive mesh dynamically adjusts with the moving reaction front inside the channel. This is illustrated in Fig. 3 using the same CO oxidation model used in the previous section. It can be seen that when the inlet temperature is increased, the reaction front where most of the inlet CO is oxidized moves close to the inlet of the channel and adaptive mesh dynamically follows. It can also be seen that the adaptive mesh places majority of points inside the reaction front where the CO concentration gradient is steep whereas the non-adaptive mesh distributes all the points uniformly regardless of steep gradients. We note that in Fig. 3, same number of MOL mesh points is used for both the solvers.

The second significant and not so obvious advantage of the above adaptive mesh technique is the automatic control of the axial integration errors in addition to the time integration errors, whereas with the standard solution method, only time integration errors are controlled. This advantage results from the decomposition of the problem into time and axial integration problems. With a non-adaptive mesh one must carefully check the accuracy of solution by varying grid resolution and ensuring that the obtained solution is grid-independent, whereas the adaptive meshing technique discussed above dynamically refines the axial mesh resolution for grid-independent solution. This is illustrated in Fig. 4 which shows the comparison of axial CO bulk gas phase concentration profiles obtained using both the adaptive and fixed mesh points. It can be seen that a finer mesh is needed when using fixed mesh to match the results of adaptive mesh. In this particular example, the fixed mesh solver needs more than three times axial mesh points than the adaptive mesh to obtain the grid-independent solution.

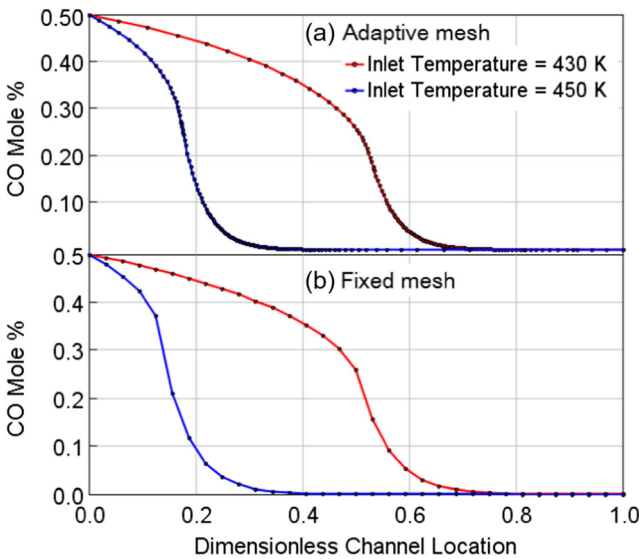

Fig. 3 CO concentration profiles demonstrating the advantage of dynamically adaptive mesh (top) over the fixed uniform mesh (bottom)

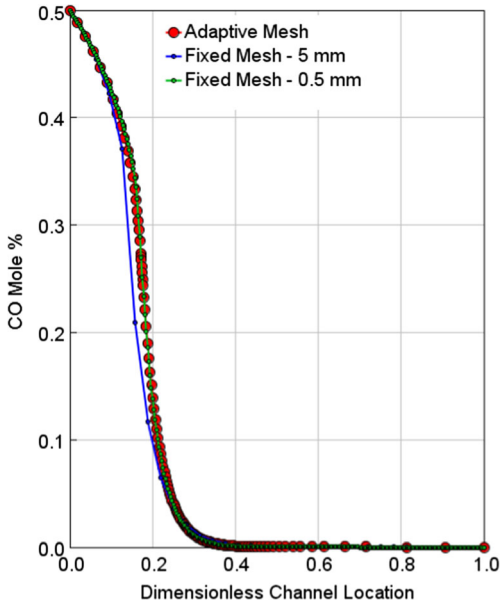

Fig. 4 CO concentration profiles demonstrating the advantage of automatic control of the axial integration errors

5 Results

In this section, we compare the results from the 1D asymptotic solution with that of 1 + 1D numerical solution for three-way catalyst (TWC), diesel oxidation catalyst (DOC), Selective Catalytic Reduction (SCR), and ammonia slip catalyst (ASC) reactors. The models used in this section are configured using published kinetic mechanisms with their full complexity and are ones commonly used in the aftertreatment modeling community. We used $\tau^{(l)} = 3, \varepsilon^{(l)} = 0.4, and\ d_{\mathrm{p}}^{(l)} = 5\mu\mathrm{m}$ for both the washcoat layers in all of the models used in this work. Figure 5 shows the bulk and effective diffusion coefficients of selected species in N_2 as a function of temperature. It can be seen from the figure that the calculated effective diffusion coefficients are on the order of $10^{-6}\mathrm{m}^2/\mathrm{s}$ which are close to the measured values reported in [20]. Thermodynamic properties of species are calculated using the polynomial coefficients obtained from the NASA database. Cordierite is used as substrate, and alumina is used as washcoat. Solid phase heat capacities and thermal conductivities as a function of temperature are calculated from lookup tables.

Since the intent of this work is to assess the accuracy of the asymptotic solution, it is important to use the same type of solution methodology for both the asymptotic and full numerical solution. For this reason, we have written the code from scratch for both the 1 + 1D and the 1D asymptotic solutions used in this work. Absolute tolerance for species fractions and coverages is set to 10^{-6}, and relative tolerance for all the other variables is set to 10^{-3}.

We note that aftertreatment reactors are generally over-designed for various practical reasons, and it is important to compare the solutions at conversion rates lower than 100%. In

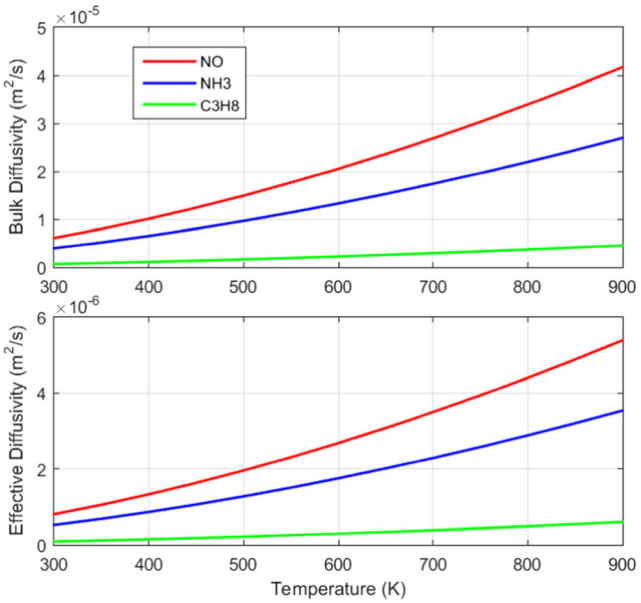

Fig. 5 Bulk and effective diffusion coefficients of selected species as a function of temperature

aftertreatment reactors, exit species conversion rates are close to 100% after the light-off, and the 100% conversion occurs in a thin reaction front somewhere inside the reactor. For fresh catalysts, this thin reaction front is generally present near the reactor inlet but moves downstream as the catalyst ages. It is possible that two different solvers may predict 100% exit conversion but with completely different axial species concentration profiles. This can be seen in Figs. 3 and 4 where exit CO conversion is 100% for both the adaptive and fixed mesh solvers even though the axial concentration profiles do not match.

The remainder of the discussion presents simulation results from four aftertreatment reactor models. TWC and DOC reactor models use a single-layer washcoat, whereas SCR and ASC reactor models use dual-layer washcoat. For each reactor, we present overall conversion and yield results based on the outlet species concentrations. We also present a limited set of washcoat concentration profiles at simulation times and axial locations that are interesting, but we strive to focus on results at higher temperatures where larger washcoat concentration gradients occur.

5.1 Single-Layer Washcoat

5.1.1 TWC

The TWC model uses the global kinetic mechanism presented in [21] which consists of 15 reactions including oxidation, reduction, water gas shift, steam reforming, and oxygen storage, and reduction reactions, and we apply it to a 50-μm-thick washcoat. We simulated a case that applied a steady temperature ramp of 12 K/min at 40,000 1/h space velocity. The inlet gas composition was fixed with lambda = 1 and consisted of 10% CO_2, 10% H_2O, 0.5% O_2, 0.2% H_2, 0.7% CO, 0.3% NO, 115 ppm C_3H_8, 450 ppm C_3H_6, and the balance N_2. Figure 6 shows the conversion of each species over time. Symbols represent the results from the 1 + 1D solution, and solid lines represent the 1D asymptotic solution. It can be seen that the light-off temperature of each species predicted by 1D asymptotic solution is as accurate as 1 + 1D solution.

Figure 7 shows select species concentration profiles at 800 s and at a normalized axial location of 0.1. It can be seen that species concentration profiles predicted by the asymptotic solution are very close to those of the numerical solution, with the largest difference of 14 ppm occurring with the CO.

5.1.2 DOC

The DOC model is constructed based on the global kinetic mechanism presented in [22] which consists of six oxidation reactions and HC adsorption and desorption to a zeolite site. A 50-μm-thick washcoat layer is used. The simulation consists of a steady temperature ramp of 9 K/min at 17,000 1/min space velocity. The inlet gas composition was fixed and consisted of 13% O_2, 5% CO_2, 5% H_2O, 500 ppm CO, 167 ppm H_2, 300 ppm NO, 330 ppm C_3H_6, 75 ppm diesel fuel, and the balance N_2. Figure 8 shows the conversion of each species over time. The HC conversion becomes negative for a short duration as the stored HC begins desorbing with increasing temperature. Symbols represent results from the 1

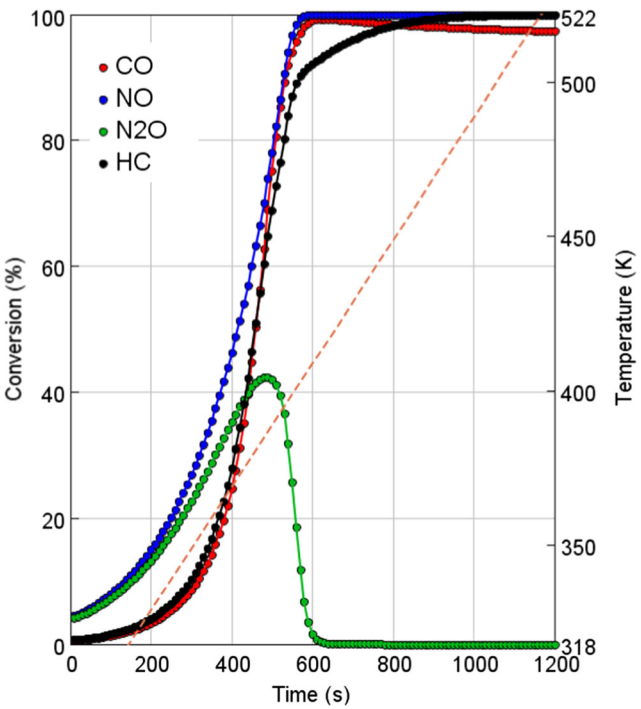

Fig. 6 Comparison of simulated exit species conversions from the 1 + 1D (symbols) and 1D asymptotic (solid lines) solvers for a TWC reactor. Inlet temperature ramp is shown on the second y-axis

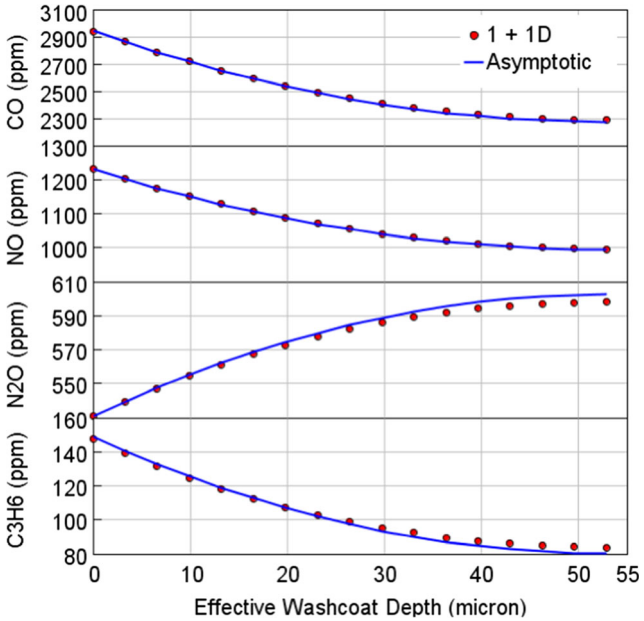

Fig. 7 Comparison of species concentration profiles within the washcoat of a TWC reactor

+ 1D solution and solid lines represent the 1D asymptotic solution. Like the TWC, no significant difference can be distinguished between the two solutions. Figure 9 shows select species concentration profiles at a normalized axial location of 0.1. The CO, C_3H_6, and NO_2 profiles come from simulation times 1200, 1100, and 1500 s, respectively. The two solutions differ by no more than 4 ppm.

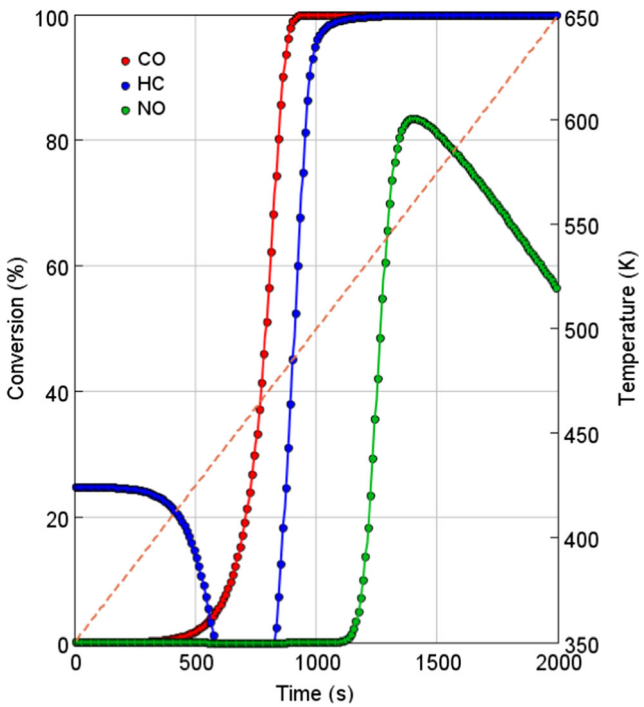

Fig. 8 Comparison of simulated exit species conversions from the 1 + 1D (symbols) and 1D asymptotic (solid lines) solutions for a DOC reactor. Inlet temperature ramp is shown on the second y-axis

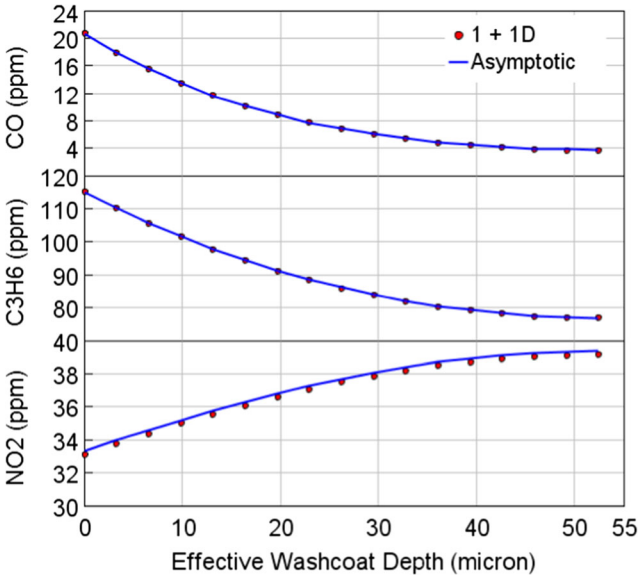

Fig. 9 Comparison of species concentration profiles within the washcoat of a DOC reactor

5.2 Dual-Layer Washcoat

5.2.1 SCR

Two groups of SCR catalysts, namely vanadia- and zeolite-based, are widely used in the exhaust gas treatment applications. The zeolite-based catalysts are active over a wider operating temperature window than the vanadia-based catalysts and are commonly used in automotive exhaust applications. Fe- and Cu-exchanged zeolite catalysts are two of the most popular catalysts for NH_3-based SCR. It is known that Fe-zeolite gives higher NO_x conversion at high temperatures, whereas Cu-zeolite yields better conversion at low temperatures. At higher temperatures (> 500 K), undesirable NH_3 oxidation reactions are faster than the desirable NO_x reduction reactions on Cu-zeolite catalyst. The difference in catalytic activity between these two catalysts with respect to temperature can be used to widen the optimum operating temperature range of SCR reactor by using dual washcoat layers. The model used in this section is constructed to simulate a dual layer SCR reactor where 25-μm-thick Fe-zeolite is deposited on top of 25-μm-thick Cu-zeolite layer. We use a global kinetic mechanism based on the one described in [23] in the top Fe-zeolite washcoat layer and a global kinetic mechanism described in [24] for the bottom Cu-zeolite layer. We simulated ten steady-state temperature cases at 60,000 1/h space velocity with inlet gas composition consisting of 8% O_2, 5% CO_2, 5% H_2O, 500 ppm NH_3, 500 ppm NO, and the balance N_2. Figure 10 shows the NO_x conversion at each steady-state temperature case for single and dual-layer washcoat configurations. It can be seen that the model correctly predicts the expected trends from both the single- and dual-layer configurations, and no significant difference exists between the 1 +

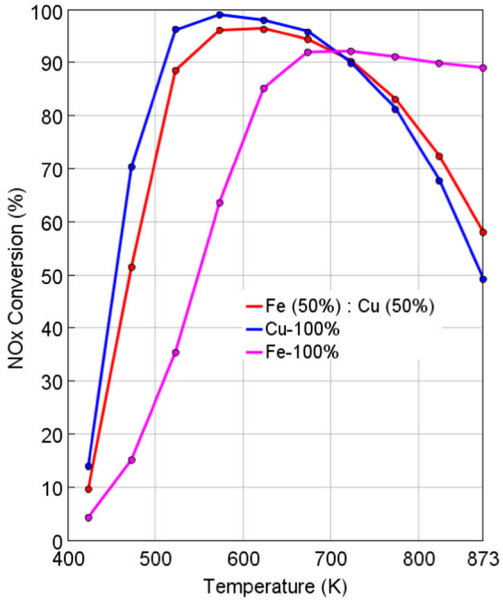

Fig. 10 Comparison of simulated NO_x conversion from the 1 + 1D (symbols) and asymptotic (solid lines) solutions as a function of inlet temperature for a SCR reactor with single- and dual-layer configurations for typical range of effective diffusivity values (~$10^{-6}m^2/s$)

1D and 1D asymptotic solutions. Figure 11 shows species concentration profiles within the washcoat for the dual-layer configuration at inlet temperature of 873 K. The species washcoat profiles are taken at a normalized axial location of 0.1. It can be seen that the asymptotic solution accurately predicts the washcoat concentration profiles.

The dual-layer SCR model is a good model for testing the limits of asymptotic solution. The asymptotic solution is derived based on the assumption of small (dimensionless) effective diffusion resistance, and it is expected that the solution accuracy degrades as diffusion resistance becomes large. As reported in [20] and also shown in Fig. 5, effective diffusivities are on the order of $10^{-6}m^2/s$ in typical aftertreatment reactors and this range is ideal for the application of the asymptotic solution. It is argued in [8] that the asymptotic solution may still give good results even when the diffusion resistance is higher. To test this argument, we arbitrarily reduced the pore diameter in this model by two orders of magnitude from 5 μm to 0.05 μm which results in effective diffusivities on the order of $10^{-7}m^2/s$. Figure 12 shows the simulated NO_x conversion for this extreme case of high pore diffusion resistance, and it can be seen that the asymptotic solution predictions match well with the 1 + 1D solution with maximum difference of 3% in NO_x conversion efficiency for the single-layer Cu-zeolite catalyst at high temperature. Figure 13 shows the washcoat concentration profiles at a normalized axial location of 0.1 for inlet temperature of 873 K.

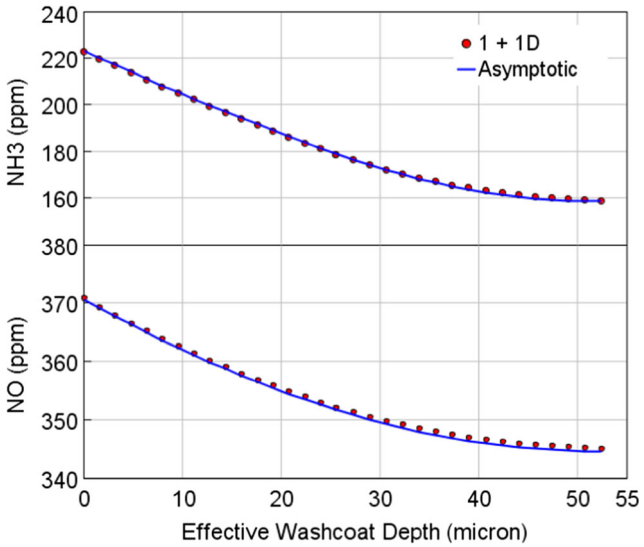

Fig. 11 Comparison of species concentration profiles within the washcoat of a dual-layer SCR reactor for typical range of effective diffusivity values (~$10^{-6}m^2/s$)

5.2.2 ASC

ASC based on platinum (Pt) is commonly used downstream of a SCR reactor to prevent the NH_3 slip from a SCR reactor. Pt catalyst selectively oxidizes the NH_3 to N_2 but also produces NO resulting in lower yields for N_2. Studies have shown that the SCR layer coated on top of Pt layer significantly reduces the NO formation resulting in higher yield for N_2 [17, 18]. In this dual-layer configuration, top SCR layer stores the NH_3 preventing the diffusion of all of the NH_3 to Pt layer and then uses it to selectively reduce the NO produced in the bottom Pt

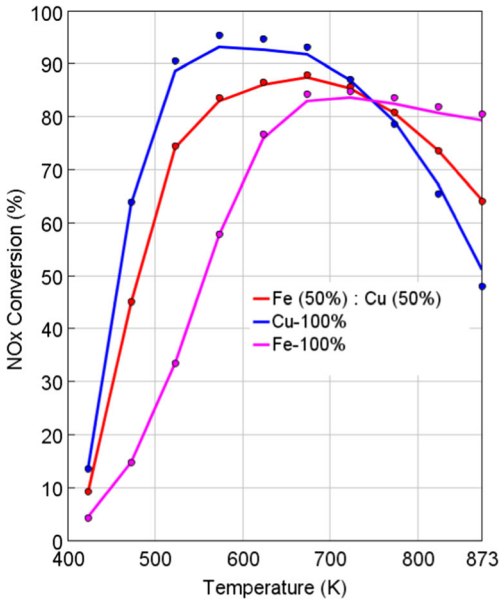

Fig. 12 Comparison of simulated NOx conversion from the 1 + 1D (symbols) and asymptotic (solid lines) solutions as a function of inlet temperature for a SCR reactor with single- and dual-layer configurations for small effective diffusivity values (~$10^{-7}m^2/s$)

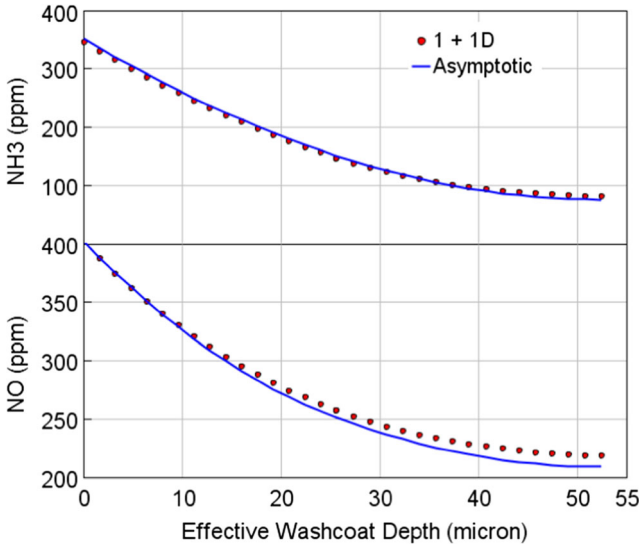

Fig. 13 Comparison of species concentration profiles within the washcoat of a dual-layer SCR reactor for small effective diffusivity values (~$10^{-7}m^2/s$)

layer to N_2. We constructed a dual-layer ASC model based on the one described in [17], which contains a 71-μm Fe-zeolite SCR washcoat layer over a 10-μm Pt washcoat layer. The global kinetics mechanism used in the Fe-zeolite layer consists of a two-site NH_3 storage mechanism based on the one described in [23], and the kinetic mechanism used in Pt layer is based on the one described in [17]. We simulated a transient case with a temperature ramp of 2 K/min at space velocity of 300,000 1/h with constant inlet gas composition consisting of 300 ppm NH_3, 6% O_2, 5% H_2O, and the balance N_2. Figure 14 shows the simulated NH_3 conversion and other species yields over time from both the solution methods. It can be seen that the asymptotic solution results accurately match the 1 + 1D results and the largest difference of about 10 ppm occurs around 6000 s in the NO yield. Figure 15 shows species concentration profiles within the washcoat at 10,000 s at a normalized axial location of 0.1. The largest difference of 6 ppm between the two solutions occurs for the NO in the Pt washcoat.

Similar to the test in the previous section, we again reduce the pore diameter by two orders of magnitude from 5 μm to 0.05 μm to test the accuracy of the asymptotic solution for small effective diffusivity values. This results in effective diffusivity values in the range of $10^{-7}m^2/s$. Figure 16 shows the simulated NH_3 conversion and other species yields over time from both the solution methods. It can be seen that the NH_3 conversion is significantly low compared to the large pore diameter case shown in Fig. 14, and the asymptotic solution accurately matches the 1 + 1D solution. From Fig. 16, it appears that the asymptotic solution gives large error in the yields of NO and N_2O, but it is noted that these species are produced in small quantities when effective diffusivities are small and the maximum discrepancy between the two solution

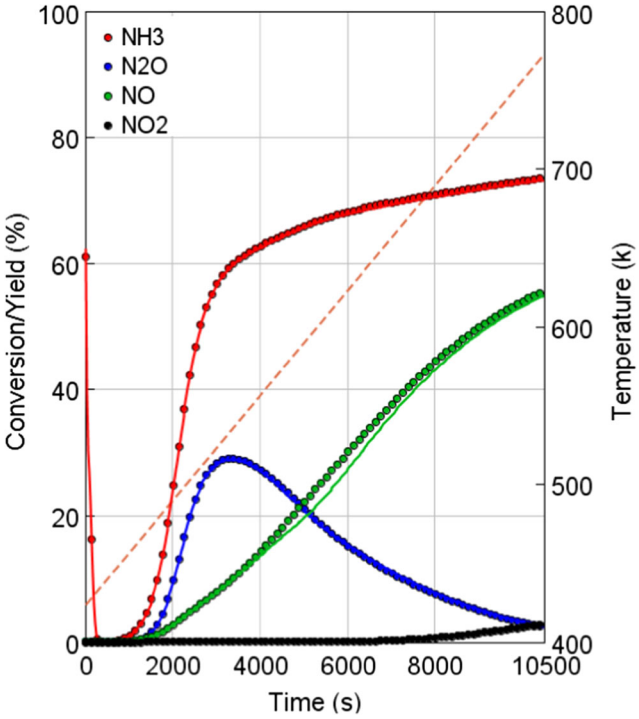

Fig. 14 Comparison of simulated exit species conversions from the 1 + 1D (symbols) and 1D asymptotic (solid lines) solvers for a dual layer ASC reactor for typical range of effective diffusivity values (~$10^{-6}m^2/s$). Inlet temperature ramp is shown on the second y-axis

methods occurs with NO around 7500 s and is about 10 ppm. Figure 17 shows species concentration profiles within the washcoat at 10,000 s at a normalized axial location of 0.1. The largest difference of about 70 ppm between the two solutions occurs for the NO in the Pt washcoat.

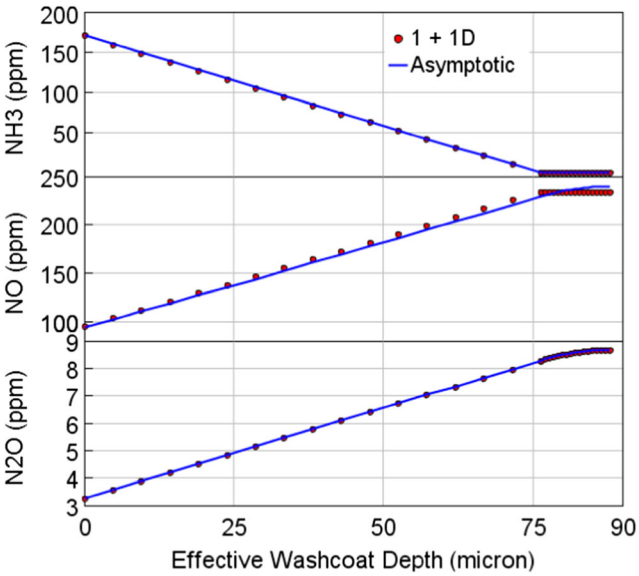

Fig. 15 Comparison of species concentration profiles within the washcoat of a dual layer ASC reactor for typical range of effective diffusivity values (~$10^{-6}m^2/s$)

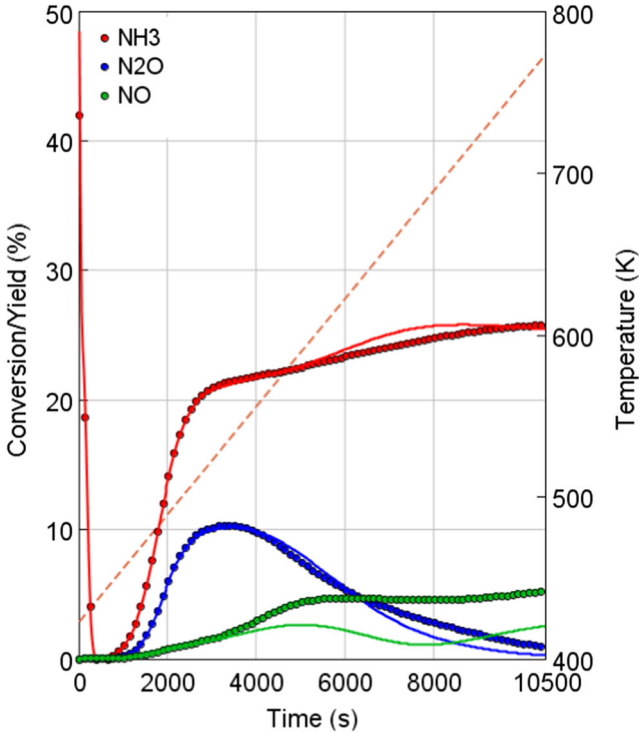

Fig. 16 Comparison of simulated exit species conversions from the 1 + 1 D (symbols) and 1D asymptotic (solid lines) solvers for a dual-layer ASC reactor for small effective diffusivity values (~$10^{-7}$$m^2$/s). Inlet temperature ramp is shown on the second y-axis

6 Summary

We have compared the predictions of the asymptotic solution with that of full 1 + 1D numerical solution for the TWC, DOC, SCR, and ASC reactor models with both single- and dual-layer washcoat configurations. The models used in the comparisons are constructed using published kinetic mechanisms with their full complexity (including non-linear reaction orders and inhibition functions) and are ones commonly used in the aftertreatment modeling community. The chosen operating conditions represent the practical range of operating conditions encountered in these reactors. We have compared the species outlet conversions as well as concentration profiles within the washcoat to assess the accuracy of the asymptotic solution and found that the asymptotic solution produces accurate results comparable to that of the full numerical solution while being computationally efficient. The asymptotic solution predictions are satisfactory with less than the 3% error in conversion efficiency even for the extreme case of high diffusion resistance where the asymptotic solution is not expected to perform well. The asymptotic solution is easy to implement and is orders of magnitude faster than the full 1 + 1D numerical solution and hence facilitates the real time simulation of models on HIL and ECU systems for the development of vehicle control strategies. Since the asymptotic solution has very little computational overhead, modelers do not have to estimate the impact of pore diffusion resistance on the results but instead always use the asymptotic solution in the aftertreatment reactor models even when pore diffusion resistance is small. As explained in the introduction, controlling regimes change with operating conditions and hence pore diffusion resistance may become important for some operating conditions for a given reactor. It will be difficult to predict a priori whether pore diffusion will be important or not for the full operating range of a reactor. Also pore diffusion cannot be ignored for the dual-layer washcoat configurations and the asymptotic solution offers significant computational savings over the 1 + 1D solution for these dual-layer washcoat applications.

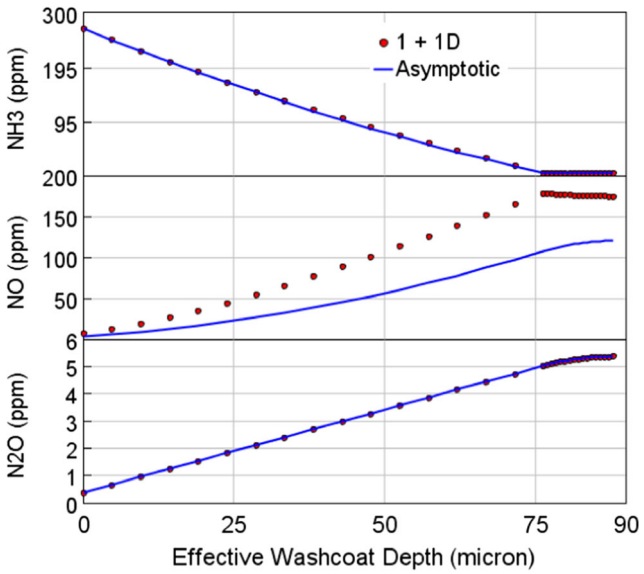

Fig. 17 Comparison of species concentration profiles within the washcoat of a dual layer ASC reactor for small effective diffusivity values (~$10^{-7}$$m^2$/s)

Acknowledgments We are grateful to Dr. Ed Bissett who spent significant amount of time discussing the asymptotic solution, adaptive meshing, and inner workings of ODE solvers. We also thank Jonathan Brown for setting up some of the models used in this work.

Compliance with Ethical Standards

Conflict of Interest On behalf of all authors, the corresponding author states that there is no conflict of interest.

References

1. Heck, R.M., Farrauto, R.J., Gulati, S.T.: Catalytic Air Pollution Control: Commercial Technology. Wiely publication (2016)
2. Joshi, S.Y., Harold, M.P., Balakotaiah, V.: Overall mass transfer coefficients and controlling regimes in catalytic monoliths. Chem. Eng. Sci. **65**, 1729–1747 (2010)
3. Metkar, P.S., Harold, M.P., Balakotaiah, V.: Experimental and kinetic modeling study of NH3-SCR of NOx on Fe-ZSM-5, Cu-chabazite and combined Fe- and Cu-zeolite monolith catalysts. Chem. Eng. Sci. **87**, 51–66 (2013)
4. Vaclavik, M., Koci, P., Novak, V., Thompsett, D.: NOx conversion and selectivity in multi-layer and sequential DOC-LNT automotive

exhaust catalysts: influence of internal transport. Chem. Eng. J. **329**, 128–134 (2017)
5. Gundlapally, S.R., Papadimitriou, I., Wahiduzzaman, S., Gu, T.: Development of ECU capable models from detailed models—application to a SCR reactor. Emission Control Science and Technology. **2**, 124–136 (2016)
6. Aris, R.: The Mathematical Theory of Diffusion And Reaction in Permeable Catalysts, Volume I, the Theory of the Steady State. Oxford University Press, London (1975)
7. Balakotaiah, V.: On the relationship between Aris and Sherwood numbers and friction and effectiveness factors. Chem. Eng. Sci. **63**, 5802–5812 (2008)
8. Bissett, E.J.: An asymptotic solution for washcoat pore diffusion in catalytic monoliths. Emission Control Science and Technology. **1**(1), 3–16 (2015a)
9. Bissett, E.J.: Small Washcoat Diffusion Resistance, Further Developments. CLEERS Workshop, Dearborn (2015b)
10. Mozaffari, B., Tischer, S., Votsmeier, M., Deutschmann, O.: A one-dimensional modeling approach for dual-layer monolith catalysts. Chem. Eng. Sci. **139**, 196–210 (2016)
11. Rink, J., Mozaffari, B., Tischer, S., Deutschmann, O., Votsmeier, M.: Real-time simulation of dual-layer converters based on the internal mass transfer coefficient approach. Top. Catal. **60**, 225–229 (2017)
12. Groppi, G., Belloli, A., Tronconi, E., Forzatti, P.: A comparison of lumped and distributed models of monolithic catalytic combustors. Chem. Eng. Sci. **50**, 2705–2715 (1995)
13. Gundlapally, S. R. (2011) Effect of non-uniform activity and conductivity on the steady-state and transient performance of catalytic reactors. PhD thesis, University of Houston
14. Gundlapally, S.R., Balakotaiah, V.: Heat and mass transfer correlations and bifurcation analysis of catalytic monoliths with developing flows. Chem. Eng. Sci. **66**(9), 1879–1892 (2011)
15. Fuller, E.N., Ensley, K., Giddings, J.C.: Diffusion of halogenated hydrocarbons in helium. The effect of structure on collision cross sections. J. Phys. Chem. **73**(11), 3679–3685 (1969)
16. Bird, R.B., Stewart, W.E., Lightfoot, E.N.: Transport Phenomena, p. 258. John Wiley and Sons, New York (1960)
17. Scheuer, A., Hauptmann, W., Drochner, A., Gieshoff, J., Vogel, H., Votsmeier, M.: Dual layer automotive ammonia oxidation catayst: experiments and computer simulation. Appl. Catal. B Environ. **111–112**, 445–455 (2012)
18. Nova, I., Colombo, M., Tronconi, E., Schmeisser, V., Bandle-Konrad, B., Zimmermann, L.: Experimental and modelling study of a dual-layer NH3 slip monolith catalyst for automotive SCR aftertreatment systems. Top. Catal. **56**, 227–231 (2013)
19. Oh, S.H., Bissett, E.J., Battiston, P.A.: Mathematical modeling of electrically heated monolith converters: model formulation, numerical method, and experimental verification. I&EC research. **32**, 1560–1567 (1993)
20. Zhang, F., Hayes, R.E., Kolaczkowski, S.T.: A new technique to measure the effective diffusivity in a catalytic monolith washcoat. Chem Eng Research and Design. **82**, 481–489 (2004)
21. Holder, R., Bollig, M., Anderson, D.R., Hochmuth, J.K.: A discussion on transport phenomena and three-way kinetics of monolithic converters. Chem. Eng. Sci. **61**(24), 8010–8027 (2006)
22. Sampara, C.S., Bissett, E.J., Chmielewski, M.: Global kinetics for a commercial diesel oxidation catalyst with two exhaust hydrocarbons. Ind. Eng. Chem. Res. **47**, 311–322 (2008)
23. Chatterjee, D., Burkhardt, T., Weibel, M., Nova, I., Grossale, A., Tronconi, E.: Numerical simulation of zeolite- and v-based SCR catalytic converters. SAE 2007–01-1136 (2007)
24. Pant, A., Schmieg, S.J.: Kinetic model of NOx SCR using urea on commercial Cu-zeolite catalyst. Ind. Eng. Chem. Res. **50**, 5490–5498 (2011)